

UAVDB: Trajectory-Guided Adaptable Bounding Boxes for UAV Detection

Yu-Hsi Chen

The University of Melbourne
Parkville, Australia

yuhsi@student.unimelb.edu.au

Abstract

The widespread deployment of Unmanned Aerial Vehicles (UAVs) in surveillance, security, and airspace management has created an urgent demand for precise, scalable, and efficient UAV detection. However, existing datasets often suffer from limited scale diversity and inaccurate annotations, hindering robust model development. This paper introduces UAVDB, a high-resolution UAV detection dataset constructed using Patch Intensity Convergence (PIC). This novel technique automatically generates high-fidelity bounding box annotations from UAV trajectory data [15], eliminating the need for manual labeling. UAVDB features single-class annotations with a fixed-camera setup and consists of RGB frames capturing UAVs across various scales, from large-scale UAVs to near-single-pixel representations, along with challenging backgrounds that pose difficulties for modern detectors. We first validate the accuracy and efficiency of PIC-generated bounding boxes by comparing Intersection over Union (IoU) performance and runtime against alternative annotation methods, demonstrating that PIC achieves higher annotation accuracy while being more efficient. Subsequently, we benchmark UAVDB using state-of-the-art (SOTA) YOLO-series detectors, establishing UAVDB as a valuable resource for advancing long-range and high-resolution UAV detection. The source code is available at <https://github.com/wish44165/UAVDB>.

1. Introduction

Precise UAV detection is critical for effective monitoring and threat response. While modern object detection algorithms, such as YOLO-series detectors [10, 11, 22, 23] and transformer-based models [2, 31], have significantly advanced UAV detection, their performance is highly dependent on high-quality annotations. Without accurate, well-annotated datasets, even SOTA models struggle with real-world UAV detection, particularly for tiny UAVs. Existing UAV datasets can be broadly categorized into two types.

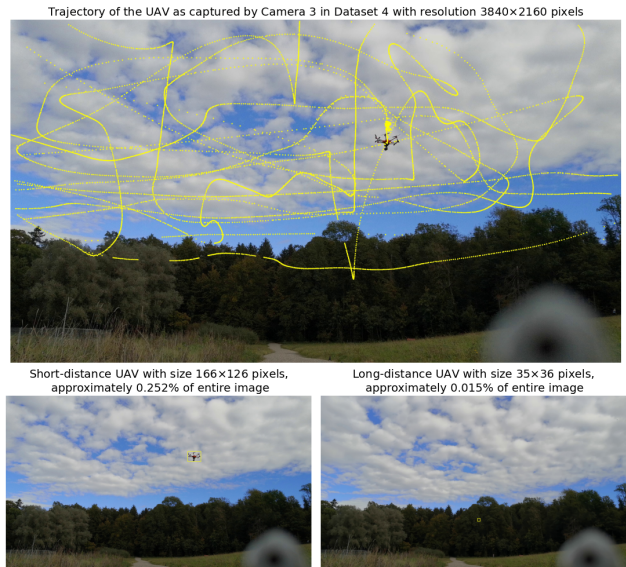


Figure 1. UAV trajectory captured by Camera 3 in Dataset 4 at 3840×2160 resolution in [15]. The yellow path represents the UAV’s trajectory. On the left, the UAV appears at a short distance with a size of 166×126 pixels, occupying approximately 0.252% of the total image area. On the right, the UAV is shown at a long distance, with a size of 35×36 pixels, covering approximately 0.015% of the entire image. This figure shows the varying visibility of the UAV depending on its distance from the camera.

The first type is ground-target UAV datasets, where UAV-mounted cameras capture objects like vehicles or pedestrians on the ground [7, 18, 24, 25, 30] and the second type is UAV-target datasets, where the UAV itself is the detection target. The latter can be further divided into three categories: 1) RGB frame with fixed-camera setup, where the camera remains stationary as presented in [17, 21], 2) RGB image with moving-camera setup, where the camera equipped on the UAV such as [14, 19], and 3) Infrared image UAV datasets, including single-frame datasets [4–6], and video-based Anti-UAV datasets [8, 9, 28, 29] which has been featured in four major challenge events.

Camera \ Dataset	1	2	3	4	5
0	5334 / 1920×1080	4377 / 1920×1080	33875 / 1920×1080	31075 / 1920×1080	20970 / 1920×1080
1	4941 / 1920×1080	4749 / 1920×1080	19960 / 1920×1080	15409 / 1920×1080	28047 / 1920×1080
2	8016 / 1920×1080	8688 / 1920×1080	17166 / 3840×2160	15678 / 1920×1080	31860 / 2704×2028
3	4080 / 1920×1080	4332 / 1920×1080	14196 / 1440×1080	10933 / 3840×2160	31992 / 1920×1080
4	–	–	18900 / 1920×1080	17640 / 1920×1080	21523 / 2288×1080
5	–	–	28080 / 1920×1080	32016 / 1920×1080	17550 / 1920×1080
6	–	–	–	11292 / 1440×1080	–

Table 1. Summary of dataset characteristics in [15]. The table displays the number of frames and resolution for each camera across different datasets. Each cell lists the number of frames followed by the resolution in pixels.

However, existing RGB frames with fixed-camera setup datasets often contain relatively large UAVs or imprecise bounding box annotations, lacking the scale diversity necessary for robust detection models. To address this, we introduce UAVDB, a high-resolution RGB frame featuring multiscale UAVs designed to improve UAV detection in diverse and complex environments. This dataset is particularly relevant for monitoring incoming UAVs from buildings or national borders using a fixed-camera setup. To construct UAVDB, we propose PIC, a technique that automatically generates accurate bounding boxes from trajectory data in [15]. Since their dataset primarily focuses on 3D UAV trajectory reconstruction with unsynchronized consumer cameras and unknown viewpoints, it lacks the precise bounding box annotations required for object detection. Fig. 1 illustrates UAV trajectories alongside human-labeled bounding boxes at different scales, highlighting the need for precise annotations. A detailed dataset structure is provided in Tab. 1. Our contributions are as follows:

1. Introduce UAVDB, a high-resolution RGB frame UAV detection dataset with multiscale UAVs and complex backgrounds, created using PIC, transforming trajectory data into high-fidelity bounding boxes, enabling automated, precise spatial annotations.
2. Provide the experiments validating PIC’s efficiency in terms of IoU and runtime, along with a comprehensive benchmark of UAVDB using SOTA YOLO-series detectors, including YOLOv8 [11], YOLOv9 [23], YOLOv10 [22], and YOLO11 [10].

2. Related Work

2.1. Object Detection by Points

Recent studies have explored point-based supervision as a cost-effective alternative to fully annotated datasets for weakly supervised object detection and instance segmentation. These approaches utilize sparse point annotations rather than full bounding boxes or masks, reducing labeling effort while guiding model learning. As shown in [3, 27], a hybrid supervision strategy combines a small subset of fully annotated images with point-labeled images, training

a point-to-box regression model to infer bounding boxes. Similarly, [12] introduces a point-guided mask representation, refining object boundaries using minimal point annotations to improve segmentation accuracy while reducing annotation costs. While point-based methods reduce labeling requirements, they face notable limitations. First, they require fine-tuning on domain-specific datasets, making them impractical for dynamic environments with shifting data distributions. Second, training-based optimization incurs considerable computational overhead, restricting their feasibility for large-scale or real-time applications. Third, weak supervision introduces spatial ambiguity, often resulting in imprecise bounding boxes, especially when object boundaries are poorly defined. These challenges underscore the need for a scalable and training-free strategy.

2.2. Bounding Box Extraction via Segmentation

Since learning-based approaches induce some inconvenience, we focus on an out-of-the-box approach to generate the bounding box annotations. As shown in Fig. 1, the goal is to extract high-fidelity bounding boxes for UAVs of varying sizes in videos only with trajectory data. A simple approach assigns a fixed bounding box around the trajectory point, but this lacks flexibility in adjusting box sizes. A more refined alternative segments the fixed size and defines the bounding box using the upper-left and lower-right corners. Image thresholding, as described in [1], is a common technique but becomes ineffective when the contrast between the UAV and background is unclear, requiring manual adjustments. Alternatively, the GrabCut algorithm [20] provides better bounding box accuracy but is computationally expensive and inefficient. Deep learning-based methods, such as DeepGrabCut [26], also demand significant computational resources. Even SOTA models like the Segment Anything Model (SAM) [13] with point prompts encounter domain-specific challenges, resulting in poor segmentation. Fig. 2 illustrates bounding boxes extracted by various methods, with a light gray (#e7e6e6 color hex) background for clearer visualization.

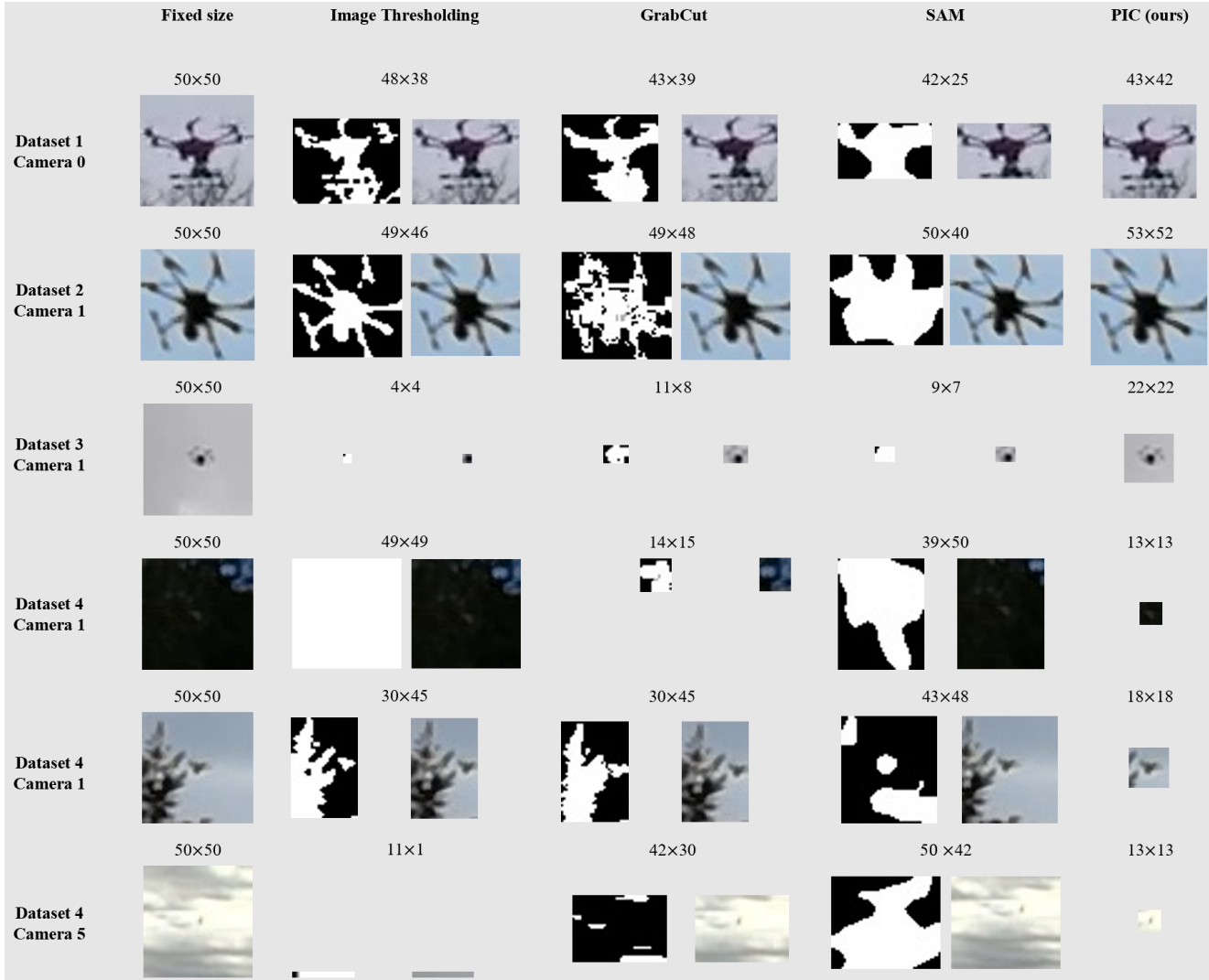


Figure 2. Comparison of bounding box extraction methods across various datasets and cameras. The rightmost column shows our PIC results, which generate high-fidelity bounding box annotations. Other columns depict results from fixed-size bounding boxes, image thresholding [1], GrabCut [20], and SAM [13]. In the last three rows, when the UAV is tiny, or the background is complex, our method remains robust, successfully extracting accurate bounding boxes even in challenging scenarios.

3. Methodology

This section presents the PIC algorithm, details the annotation process, and introduces the UAVDB dataset.

3.1. Patch Intensity Convergence (PIC)

The PIC technique extracts UAV bounding boxes from trajectory annotations via an adaptive inward-outward expansion, ensuring efficient localization without relying on external models or predefined dimensions. The process consists of four steps: initialization, iterative expansion, patch intensity calculation, and convergence assessment.

3.1.1. Initialization

Given a trajectory point (x_0, y_0) , the bounding box is initialized as a square region B_0 of size $w_0 \times h_0$:

$$B_0 = \{(x, y) \mid x_0 - w_0/2 \leq x \leq x_0 + w_0/2, \\ y_0 - h_0/2 \leq y \leq y_0 + h_0/2\}.$$

3.1.2. Iterative Expansion

The bounding box expands outward by a fixed step δ in all directions per iteration:

$$w_{t+1} = w_t + \delta, \quad h_{t+1} = h_t + \delta.$$

The expanded region B_{t+1} captures a progressively larger area around the trajectory point.

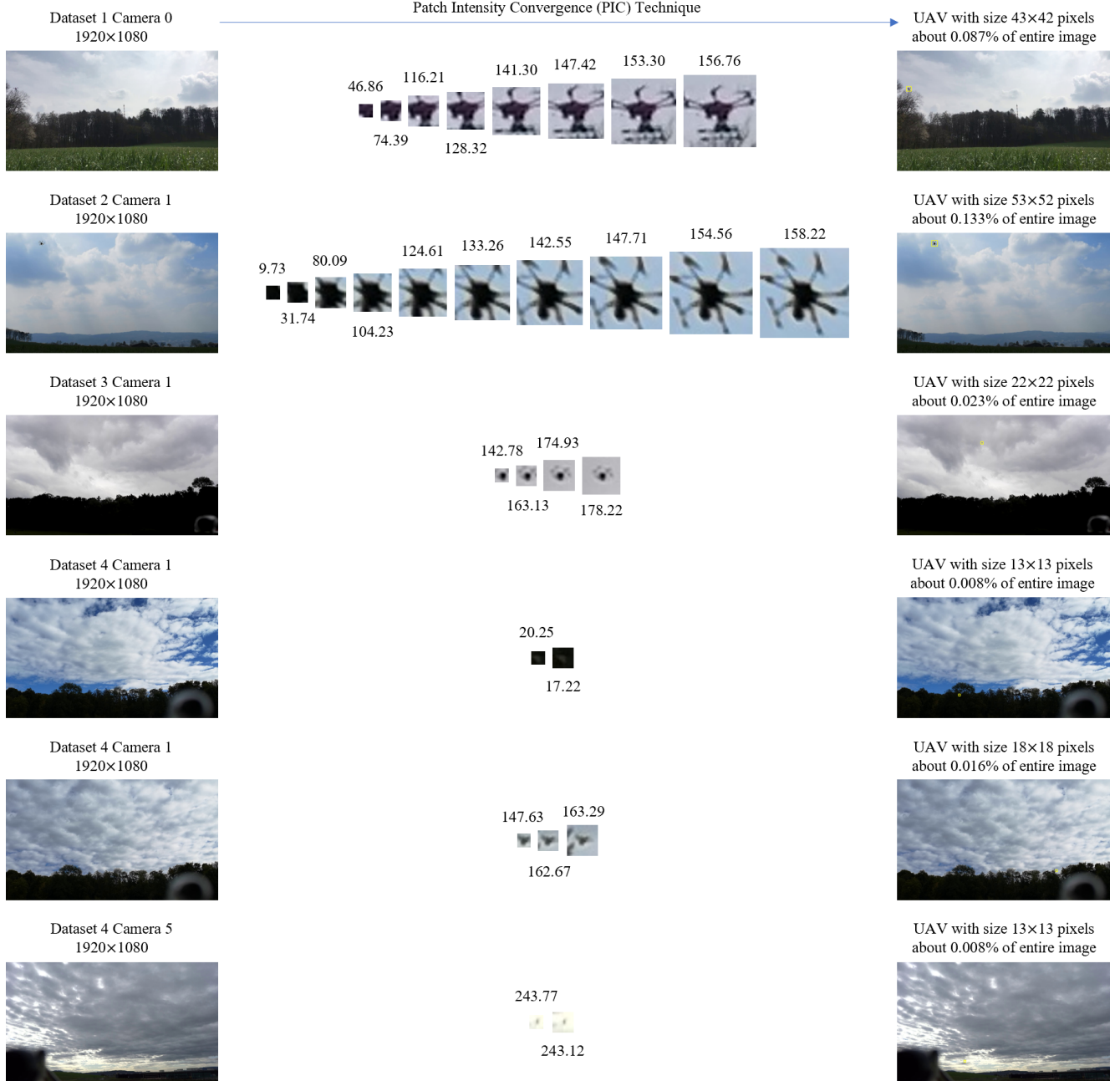


Figure 3. Stepwise demonstration of the PIC technique applied across various datasets and cameras. The middle columns illustrate the iterative bounding box expansion centered on the UAV, with corresponding pixel intensity values. The rightmost column presents the final PIC annotations along with UAV size and aspect ratio in each scenario.

3.1.3. Patch Intensity Calculation

At each step, the mean pixel intensity inside the bounding box is computed as:

$$\mu_t = \frac{1}{|B_t|} \sum_{(x,y) \in B_t} I(x,y).$$

where $I(x,y)$ denotes the pixel intensity at (x,y) .

3.1.4. Convergence Assessment

Expansion halts when the intensity change between consecutive iterations falls below a threshold ϵ :

$$|\mu_{t+1} - \mu_t| < \epsilon.$$

This criterion ensures that further expansion does not significantly contribute to capturing UAV-relevant pixels, mark-

Camera \ Dataset	1	2	3	4
0	train / 291	test / 237	train / 3190	test / 2355
1	valid / 303	train / 343	train / 841	train / 416
2	train / 394	train / 809	valid / 1067	train / 701
3	test / 348	valid / 426	train / 638	train / 727
4	-	-	test / 1253	valid / 924
5	-	-	train / 1303	train / 1110
6	-	-	-	test / 385

Table 2. Overview of the UAVDB constructed using the proposed PIC approach. The table shows the distribution of images across different datasets and camera configurations, specifying the number of images used for training, validation, and testing.

ing the final bounding box boundary.

We apply the PIC technique to the videos and trajectory data from [15], using an initial patch size of $w_0 = h_0 = 8$ pixels, an expansion step of $\delta = 5$ pixels, and a convergence threshold of $\epsilon = 4$. For UAVDB, we extract one frame per ten frames (around 10% of the footage) from Tab. 1 to construct the database. The resulting dataset consists of 10,763 training images, 2,720 validation images, and 4,578 test images, as detailed in Tab. 2. Since Dataset 5 in [15] lacks 2D trajectory information, we serve as an unseen scenario, with its detection results presented in the experimental section. Notably, our framework allows flexible adjustment of the extraction rate to generate larger or smaller datasets. Fig. 3 illustrates the stepwise expansion of PIC across different datasets, demonstrating its precision in challenging scenarios. The middle columns depict the incremental bounding box expansions with corresponding pixel intensity values. The rightmost column shows a reference image indicating UAV size as a percentage of the total image area. PIC accurately localizes UAVs across scales, from large (53×52 pixels around 0.133% of the image) to tiny (13×13 pixels around 0.008% of the image), providing the comprehensive and high-fidelity bounding box annotations.

4. Experimental Results

We first evaluate the effectiveness of the proposed PIC approach in terms of IoU metrics and runtime efficiency compared to other methods. We then present comprehensive benchmark results on UAVDB.

4.1. Annotation Accuracy and Runtime Efficiency

First, human-labeled bounding boxes are considered ground truth annotations. For the fixed-size and thresholding [1] approaches, we use a 50×50 region size and set the threshold value to 150, based on empirical testing, which yields the best performance. For the GrabCut [20] and Segment Anything Model (SAM) [13] approaches, we use the OpenCV package and the ViT-B pre-trained SAM model, respectively. As shown in Tab. 3, the PIC approach outperforms other methods, achieving the highest IoU while

Methods	Average IoU	Runtime
human-labeled	1.000	19.00
Fixed-size	0.278	0.007
Thresholding [1]	0.316	0.009
GrabCut [20]	0.425	2.423
SAM [13]	0.249	0.484
PIC (ours)	0.464	0.007

Table 3. Comparison of different UAV bounding box extraction methods regarding average IoU and runtime (seconds).

maintaining a minimal runtime of 0.007 seconds, comparable to the fixed-size method. This demonstrates that the computational time of the PIC process is negligible compared to image reading and output. In contrast, despite its advanced segmentation capabilities, SAM struggles with UAV-specific challenges, resulting in the lowest IoU. This illustrates that SAM cannot generalize effectively without retraining on a specific dataset. These results highlight the effectiveness of PIC in providing both accurate and computationally efficient UAV bounding box extraction, making it ideal for large-scale and real-time applications.

4.2. Benchmark on UAVDB

To benchmark the proposed UAVDB, we evaluate several SOTA detectors, including YOLOv8 [11], YOLOv9 [23], YOLOv10 [22], and YOLO11 [10]. These detectors were trained on 10,763 training images, 2,720 validation images, and 4,578 test images from UAVDB, as shown in Tab. 2. The experiments were conducted on a high-performance computing (HPC) system [16], utilizing an NVIDIA A100 GPU with 80 GB of memory. All models were trained with an image size of 640, a batch size of 32, 100 epochs, and eight workers. Mosaic augmentation was applied throughout training, excluding the final 10 epochs. Additionally, we fine-tuned the models using officially released pre-trained weights. Tab. 4 summarizes the training time, inference time, number of model parameters, FLOPs, and average precision (AP) for both validation and test results for each detector. Further, validation performance across epochs is illustrated in Fig. 4. Fig. 5 showcases the predictions made by the YOLO11s model on Dataset 5, which includes scenarios not present in the training data, highlighting the model’s ability to handle previously unseen situations. The detection results closely match the UAV sizes, validating the high fidelity of the bounding box annotations in UAVDB. Incorporating these high-quality predicted bounding boxes into the training set can further enhance the model’s capability to detect UAVs in various scenarios.

4.3. Discussion

As shown in Tab. 3, the human-labeled approach requires an average of 19 seconds per annotation, including zoom-

Model	Training Time (hours:mins:sec)	Inference Time (per image, ms)	#Param. (M)	FLOPs (G)	AP_{50}^{val}	AP_{50-95}^{val}	AP_{50}^{test}	AP_{50-95}^{test}
YOLOv8n	01:40:31	0.9	2.7	6.8	0.829	0.522	0.789	0.450
YOLOv8s	01:55:05	1.2	9.8	23.3	0.814	0.545	0.796	0.450
YOLOv8m	02:43:08	1.8	23.2	67.4	0.809	0.538	0.827	0.526
YOLOv8l	03:54:44	2.6	39.4	145.2	0.830	0.563	0.836	0.544
YOLOv8x	04:33:08	3.5	61.6	226.7	0.820	0.554	0.728	0.448
YOLOv9t	02:53:11	2.5	2.6	10.7	0.839	0.501	0.848	0.508
YOLOv9s	03:05:02	2.6	9.6	38.7	0.819	0.517	0.834	0.484
YOLOv9m	05:08:28	4.1	32.6	130.7	0.840	0.507	0.858	0.522
YOLOv9c	06:17:08	5.3	50.7	236.6	0.851	0.544	0.851	0.504
YOLOv9e	08:00:05	6.6	68.5	240.7	0.755	0.414	0.768	0.383
YOLOv10n	02:05:39	0.7	2.7	8.2	0.764	0.492	0.731	0.417
YOLOv10s	02:23:03	1.2	8.0	24.4	0.817	0.530	0.823	0.516
YOLOv10m	03:06:59	1.8	16.5	63.4	0.798	0.531	0.821	0.536
YOLOv10b	03:29:18	2.1	20.4	97.9	0.801	0.517	0.760	0.467
YOLOv10l	04:04:22	2.5	25.7	126.3	0.774	0.502	0.842	0.517
YOLOv10x	05:14:07	3.5	31.6	169.8	0.771	0.507	0.693	0.431
YOLO11n	01:50:00	0.9	2.6	6.3	0.847	0.527	0.856	0.539
YOLO11s	02:07:01	1.2	9.4	21.3	0.826	0.553	0.885	0.578
YOLO11m	03:07:40	1.9	20.0	67.6	0.827	0.588	0.843	0.578
YOLO11l	04:09:45	2.4	25.3	86.6	0.810	0.555	0.798	0.517
YOLO11x	05:20:38	3.6	56.8	194.4	0.812	0.560	0.782	0.534

Table 4. Performance metrics of YOLOv8 [11], YOLOv9 [23], YOLOv10 [22], and YOLO11 [10] models trained on UAVDB.

ing and detailed adjustments, which is time-consuming and labor-intensive, particularly for large datasets with tiny objects. In contrast, our PIC approach is approximately $2700\times$ faster, though with a slight sacrifice in accuracy. Despite this, the proposed dataset has proven effective in training detectors, as demonstrated by the visualizations in Fig. 5. While the PIC method performs well on current datasets, we acknowledge that low-altitude UAV flights, with cluttered and rapidly changing backgrounds, may pose challenges. In such dynamic environments, local intensity variations could impact the pixel intensity metric for bounding box expansion. However, the adaptive nature of PIC, focusing on local intensity changes, allows it to handle moderate background texture variations. Further improvements could be explored for highly dynamic scenarios, such as incorporating multi-frame temporal information or background subtraction, to enhance robustness further and ensure consistent performance for the PIC technique.

5. Conclusion

In this paper, we introduced UAVDB, a high-quality dataset with precise bounding box annotations facilitated by our proposed PIC technique. PIC is an intuitive, efficient, and innovative method that enables automated, high-accuracy spatial annotations without manual labeling effort. UAVDB addresses critical limitations in existing UAV datasets, such

as the lack of accurate annotations and insufficient environmental diversity, significantly enhancing the applicability of detection algorithms in real-world scenarios. Through IoU and runtime evaluations, alongside benchmarking SOTA YOLO detectors, we demonstrated the versatility of both UAVDB and the PIC approach under varied conditions. These results validate UAVDB as a valuable resource for advancing UAV detection technologies. Looking forward, the adaptability of PIC presents exciting opportunities for future work. Its lightweight design could be further enhanced by incorporating multi-frame temporal information or background subtraction to improve robustness in dynamic environments. The flexibility to fine-tune PIC for specific domains ensures its continued scalability and relevance across various UAV detection applications. As UAV detection technology progresses, UAVDB and PIC provide a solid foundation for advancing real-time, large-scale UAV detection in diverse environments.

6. Acknowledgments

We thank the Photogrammetry and Remote Sensing group at ETH Zurich for their invaluable contribution to the multi-view drone tracking dataset [15], which features high-resolution UAV video and 2D trajectory data.

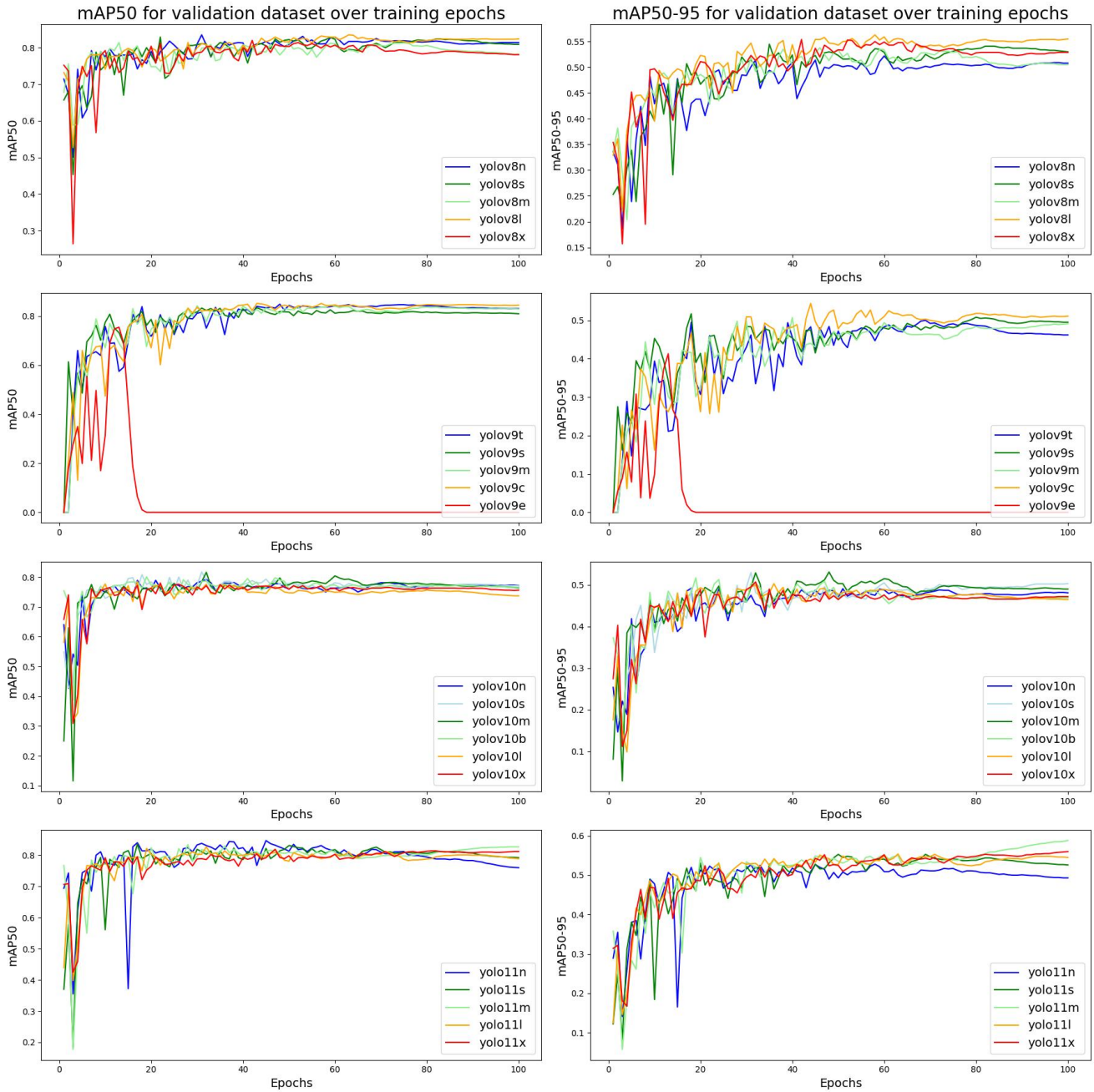


Figure 4. Validation performance of YOLOv8 [11], YOLOv9 [23], YOLOv10 [22], and YOLO11 [10] models over training epochs.

References

- [1] Salem Saleh Al-Amri, Namdeo V Kalyankar, et al. Image segmentation by using threshold techniques. *arXiv preprint arXiv:1005.4020*, 2010. 2, 3, 5
- [2] Nicolas Carion, Francisco Massa, Gabriel Synnaeve, Nicolas Usunier, Alexander Kirillov, and Sergey Zagoruyko. End-to-end object detection with transformers. In *European conference on computer vision*, pages 213–229. Springer, 2020. 1
- [3] Liangyu Chen, Tong Yang, Xiangyu Zhang, Wei Zhang, and Jian Sun. Points as queries: Weakly semi-supervised object detection by points. In *Proceedings of the IEEE/CVF conference on computer vision and pattern recognition*, pages 8823–8832, 2021. 2
- [4] Yimian Dai, Yiquan Wu, Fei Zhou, and Kobus Barnard. Attentional Local Contrast Networks for Infrared Small Target Detection. *IEEE Transactions on Geoscience and Remote Sensing*, pages 1–12, 2021. 1

Camera 0 in Dataset 5 with resolution 1920×1080 pixels



Camera 1 in Dataset 5 with resolution 1920×1080 pixels



Camera 2 in Dataset 5 with resolution 2704×2028 pixels



Camera 3 in Dataset 5 with resolution 1920×1080 pixels



Camera 4 in Dataset 5 with resolution 2288×1080 pixels



Camera 5 in Dataset 5 with resolution 1920×1080 pixels



Figure 5. Detection results predicted by YOLO11s on unseen scenarios.

- [5] Yimian Dai, Yiquan Wu, Fei Zhou, and Kobus Barnard. Asymmetric contextual modulation for infrared small target detection. In *IEEE Winter Conference on Applications of Computer Vision, WACV 2021*, 2021.
- [6] Yimian Dai, Xiang Li, Fei Zhou, Yulei Qian, Yaohong Chen, and Jian Yang. One-Stage Cascade Refinement Networks for Infrared Small Target Detection. *IEEE Transactions on Geoscience and Remote Sensing*, pages 1–17, 2023. 1
- [7] Jian Ding, Nan Xue, Gui-Song Xia, Xiang Bai, Wen Yang, Michael Ying Yang, Serge Belongie, Jiebo Luo, Mihai Datcu, Marcello Pelillo, et al. Object detection in aerial images: A large-scale benchmark and challenges. *IEEE transactions on pattern analysis and machine intelligence*, 44(11): 7778–7796, 2021. 1
- [8] Bo Huang, Jianan Li, Junjie Chen, Gang Wang, Jian Zhao, and Tingfa Xu. Anti-uav410: A thermal infrared benchmark and customized scheme for tracking drones in the wild. *T-PAMI*, 2023. 1
- [9] Nan Jiang, Kuiran Wang, Xiaoke Peng, Xuehui Yu, Qiang Wang, Junliang Xing, Guorong Li, Qixiang Ye, Jianbin Jiao, Zhenjun Han, et al. Anti-uav: a large-scale benchmark for vision-based uav tracking. *T-MM*, 2021. 1
- [10] Glenn Jocher and Jing Qiu. Ultralytics yolo11, 2024. 1, 2, 5, 6, 7
- [11] Glenn Jocher, Ayush Chaurasia, and Jing Qiu. YOLO by Ultralytics, 2023. 1, 2, 5, 6, 7
- [12] Beomyoung Kim, Joonhyun Jeong, Dongyoon Han, and Sung Ju Hwang. The devil is in the points: Weakly semi-supervised instance segmentation via point-guided mask representation. In *Proceedings of the IEEE/CVF Conference on Computer Vision and Pattern Recognition*, pages 11360–11370, 2023. 2
- [13] Alexander Kirillov, Eric Mintun, Nikhila Ravi, Hanzi Mao, Chloe Rolland, Laura Gustafson, Tete Xiao, Spencer Whitehead, Alexander C Berg, Wan-Yen Lo, et al. Segment anything. In *Proceedings of the IEEE/CVF International Conference on Computer Vision*, pages 4015–4026, 2023. 2, 3, 5
- [14] Jing Li, Dong Hye Ye, Timothy Chung, Mathias Kolsch, Juan Wachs, and Charles Bouman. Multi-target detection and tracking from a single camera in unmanned aerial vehicles (uavs). In *2016 IEEE/RSJ international conference on intelligent robots and systems (IROS)*, pages 4992–4997. IEEE, 2016. 1
- [15] Jingtong Li, Jesse Murray, Dorina Ismaili, Konrad Schindler, and Cenek Albl. Reconstruction of 3d flight trajectories from ad-hoc camera networks. In *2020 IEEE/RSJ International Conference on Intelligent Robots and Systems (IROS)*, pages 1621–1628. IEEE, 2020. 1, 2, 5, 6
- [16] Bernard Meade, Lev Lafayette, Greg Sauter, and Daniel Tosello. Spartan hpc-cloud hybrid: delivering performance and flexibility. *University of Melbourne*, 10:49, 2017. 5
- [17] Maciej Pawelczyk and Marek Wojtyra. Real world object detection dataset for quadcopter unmanned aerial vehicle detection. *IEEE Access*, 8:174394–174409, 2020. 1
- [18] Sebastien Razakarivony and Frederic Jurie. Vehicle detection in aerial imagery: A small target detection benchmark. *Journal of Visual Communication and Image Representation*, 34:187–203, 2016. 1
- [19] AWS Open Data Registry. Airborne object tracking dataset, 2023. Accessed: Feb. 19, 2025. 1
- [20] Carsten Rother, Vladimir Kolmogorov, and Andrew Blake. ” grabcut” interactive foreground extraction using iterated graph cuts. *ACM transactions on graphics (TOG)*, 23(3): 309–314, 2004. 2, 3, 5
- [21] Daniel Steininger, Verena Widhalm, Julia Simon, Andreas Kriegler, and Christoph Sulzbachner. The aircraft context dataset: Understanding and optimizing data variability in aerial domains. In *Proceedings of the IEEE/CVF International Conference on Computer Vision*, pages 3823–3832, 2021. 1
- [22] Ao Wang, Hui Chen, Lihao Liu, Kai Chen, Zijia Lin, Jungong Han, and Guiguang Ding. Yolov10: Real-time end-to-end object detection. *arXiv preprint arXiv:2405.14458*, 2024. 1, 2, 5, 6, 7
- [23] Chien-Yao Wang, I-Hau Yeh, and Hong-Yuan Mark Liao. Yolov9: Learning what you want to learn using programmable gradient information. *arXiv preprint arXiv:2402.13616*, 2024. 1, 2, 5, 6, 7
- [24] Jinwang Wang, Wen Yang, Haowen Guo, Ruixiang Zhang, and Gui-Song Xia. Tiny object detection in aerial images. In *2020 25th international conference on pattern recognition (ICPR)*, pages 3791–3798. IEEE, 2021. 1
- [25] Chang Xu, Jinwang Wang, Wen Yang, Huai Yu, Lei Yu, and Gui-Song Xia. Detecting tiny objects in aerial images: A normalized wasserstein distance and a new benchmark. *ISPRS Journal of Photogrammetry and Remote Sensing*, 190: 79–93, 2022. 1
- [26] Ning Xu, Brian Price, Scott Cohen, Jimei Yang, and Thomas Huang. Deep grabcut for object selection. *arXiv preprint arXiv:1707.00243*, 2017. 2
- [27] Shilong Zhang, Zhuoran Yu, Liyang Liu, Xinjiang Wang, Aojun Zhou, and Kai Chen. Group r-cnn for weakly semi-supervised object detection with points. In *Proceedings of the IEEE/CVF conference on computer vision and pattern recognition*, pages 9417–9426, 2022. 2
- [28] Jian Zhao, Gang Wang, Jianan Li, Lei Jin, Nana Fan, Min Wang, Xiaojuan Wang, Ting Yong, Yafeng Deng, Yandong Guo, et al. The 2nd anti-uav workshop & challenge: methods and results. *arXiv preprint arXiv:2108.09909*, 2021. 1
- [29] Jian Zhao, Jianan Li, Lei Jin, Jiaming Chu, Zhihao Zhang, Jun Wang, Jiangqiang Xia, Kai Wang, Yang Liu, Sadaf Gulshad, et al. The 3rd anti-uav workshop & challenge: Methods and results. *arXiv preprint arXiv:2305.07290*, 2023. 1
- [30] Pengfei Zhu, Longyin Wen, Dawei Du, Xiao Bian, Heng Fan, Qinghua Hu, and Haibin Ling. Detection and tracking meet drones challenge. *IEEE Transactions on Pattern Analysis and Machine Intelligence*, 44(11):7380–7399, 2021. 1
- [31] Xizhou Zhu, Weijie Su, Lewei Lu, Bin Li, Xiaogang Wang, and Jifeng Dai. Deformable detr: Deformable transformers for end-to-end object detection. *arXiv preprint arXiv:2010.04159*, 2020. 1